



Preparation and luminescence properties of $\text{WO}_3:\text{Eu}^{3+}@\text{SiO}_2$ nanocomposites

DONG LIANG^{1,2}, SANG XIONG^{2,3,*} , XIAOMENG ZHANG^{1,2}, YUANFENG YE¹, JINGXIN CAO¹, XINGXING HU¹, YAO SONG¹ and QIANWEN WEI¹

¹ College of Materials Engineering, Jinling Institute of Technology, Nanjing 211167, Jiang Su, People's Republic of China

² Jiangsu Key Laboratory of Advanced Structural Materials and Application Technology, Nanjing 211167, Jiang Su, People's Republic of China

³ College of Materials Science and Engineering, Nanjing Institute of Technology, Nanjing 211167, Jiang Su, People's Republic of China

*Author for correspondence (xionsang@njit.edu.cn)

MS received 7 September 2022; accepted 14 December 2022

Abstract. $\text{WO}_3:\text{Eu}^{3+}$ powder was prepared by microemulsion method with cetyltrimethyl ammonium bromide (CTAB) as a surfactant. The prepared $\text{WO}_3:\text{Eu}^{3+}$ samples were wrapped with SiO_2 by a coating method. The $\text{WO}_3:\text{Eu}^{3+}@\text{SiO}_2$ nanocomposites with the core-shell structure were prepared by controlling tetraethyl orthosilicate (TEOS) content (1, 3, 5 and 7%) and water-alcohol ratio (1:3, 1:1.5, 1:1 and 2:1). The structure, morphology and luminescence properties of the prepared $\text{WO}_3:\text{Eu}^{3+}@\text{SiO}_2$ samples were characterized by XRD, SEM, TEM and fluorescence spectra. The results show that the prepared $\text{WO}_3:\text{Eu}^{3+}@\text{SiO}_2$ nanocomposites are spherical and granular, and the average particle size is below 100 nm. Under the condition of different TEOS contents, the strongest characteristic peak is located at 554 nm in the green light band at the excitation wavelength of 328 nm. Among the different water-alcohol ratio conditions, the prepared $\text{WO}_3:\text{Eu}^{3+}@\text{SiO}_2$ nanocomposite has the strongest luminescence intensity at the water-alcohol ratio of 1:3, and the excitation wavelength is 328 nm. The excitation spectra measured at 612 nm have prominent characteristic peaks at 362, 394, 422, 465 and 499 nm, which correspond to the transition of ${}^7\text{F}_0\rightarrow{}^5\text{D}_4$, ${}^7\text{F}_0\rightarrow{}^5\text{L}_6$, ${}^7\text{F}_0\rightarrow{}^5\text{D}_3$, ${}^7\text{F}_0\rightarrow{}^5\text{D}_2$ and ${}^7\text{F}_0\rightarrow{}^5\text{D}_1$, respectively.

Keywords. Microemulsion method; tungsten oxide; coating method; luminous intensity.

1. Introduction

In the past few years, more and more attention has been paid to the achievements of designing catalysts on the nanoscale. Continuous research by scientists has succeeded in producing an ability to synthesize new materials and perform new functions, and some important achievements have been made. For example, sol-based units of palladium cores and ornamentals assemble nanoparticles $\text{Pd}@\text{CeO}_2$ [1]. A unique methane combustion catalyst is produced when they are uniformly deposited on a functionalized alumina carrier [2]. Core-shell structures such as precious metals (silver, gold, palladium and platinum) particles in carbon spheres [3], $\text{Pt}@\text{CoO}$ yolk/shell nanoparticles [4], $\text{Pt}@\text{mSiO}_2$ [5] and Au nanoparticles in hollow ZrO_2 and hollow SiO_2 spheres constitute a broad class of nanoengineered catalysts. In cases where the solid metal core is encapsulated in an oxide shell, the goal is usually to isolate the metal particles from each other to avoid sintering while maintaining the accessibility of the active point. In the past decade, significant efforts have been made to prepare mesoporous core-shell nanomaterials

for their potential applications in drug delivery vectors [6], optical bioprobes, sensors [7] and biomedicine. Dou *et al* [8] synthesized a new structure of silver shell gold nanorods modified by $\text{BaGdF}_5:\text{Yb}^{3+}$ and Er^{3+} nanoparticles through a simple method. Coating silver shells increased the biological stability of AuNRs, and AuNR@Ag nanoparticles could be used as excellent surface-enhanced Raman scattering probes. Lin *et al* [9] studied and synthesized new core-shell MOFs/CDs@OCMC nanoparticles with fluorescence characteristics, and evaluated the diagnosis and treatment of cancer.

Tungsten oxide (WO_3) is an important semiconductor functional material. Nanoscale WO_3 has a unique role because of its large specific surface areas, such as catalysis, stealth properties and other applications [10–12]. Gorobtsov *et al* [13] studied the synthesis of nanoscale WO_3 by oxalic acid chemical precipitation. Deepa and Rajendran [14] prepared tungsten trioxide nanopowders using CTAB/n-cloth/octane/ H_2O microemulsion system, Na_2WO_4 and hydrochloric acid as raw materials. The structure, size and morphology of tungsten trioxide nanoparticles were characterized by an X-ray diffractometer (XRD) and transmission

electron microscope (TEM). Nano-SiO₂ has a large specific surface area, a small size effect and excellent optical and electrical properties, so it is widely used in rubber products, colours, catalysts, medical carriers and other fields [15]. Khosravi *et al* [16] oxidized cyclohexane to cyclohexanone (Ke) and cyclohexanol (Al) using a new type of highly efficient magnetic ZrFe₂O₄@SiO₂-TCPP nanocatalyst. Mesoporous ZrFe₂O₄ nanoparticles with nanometre structure were synthesized by solvothermal method, and ZrFe₂O₄@SiO₂ core-shell was prepared by wrapping silica with TEOS. There are two popular methods for the preparation of mNPs(metal oxide)/SiO₂ materials: the coating method and the deposition method [17–21]. mNPs are firstly prepared by the coating method, and then the surface of metal oxide is chemically modified to inhibit its agglomeration and improve the compatibility with SiO₂. Finally, the modified metal oxide is used as a template to catalyse the hydrogen condensation of ethyl TEOS with an alkaline catalyst to form the Si–O–Si network to realize the metal oxide coating. That is the mNPs@SiO₂ materials. However, the photocatalytic performance of traditional WO₃ materials is not excellent, so it is necessary to modify the surface of WO₃ to improve the photocatalytic activity. SiO₂ is a good coating material. SiO₂ is used as composite shell material because of the high stability of silica gel in a liquid medium, nanoshell structure and controllable shell thickness in the deposition process. As a new type of functional material, nanocomposite materials show excellent application potential in various fields and have become a hot topic in the research of nanocomposite materials. Based on the advantages of SiO₂ and WO₃ nanoparticles, this study intends to prepare WO₃:Eu³⁺@SiO₂ nanoparticles to improve the performance of WO₃.

In this study, using europium nitrate and ammonium tungstate as precursors, WO₃:Eu³⁺ powder was prepared by microemulsion method with cetyltrimethyl ammonium bromide (CTAB) as the surfactant. The prepared WO₃:Eu³⁺ samples were wrapped with SiO₂ by a coating method, and nanocomposites were prepared by controlling TEOS content at 1, 3, 5 and 7%. The WO₃:Eu³⁺@SiO₂ core-shell structure was prepared by controlling the water–alcohol ratio at 1:3, 1:1.5, 1:1 and 2:1. The structure, morphology and luminescence properties of the prepared WO₃:Eu³⁺@SiO₂ samples were characterized by XRD, SEM (scanning electron microscope), TEM and fluorescence spectra. The optimum TEOS content and the ratio of water to alcohol were analysed synthetically.

2. Experimental

2.1 Raw materials

Europium nitrate (Eu(NO₃)₃·6H₂O) produced by Shanghai Aladdin Biochemical Technology Co., LTD was used. Ammonium paratungstate ((NH₄)₁₀H₂(W₂O₇)₆·xH₂O) produced by Shanghai Aladdin Biochemical Technology Co.,

LTD was used. Hexadecyl trimethyl ammonium bromide (CTAB, C₁₂H₄₂NBr) as surfactant and *n*-butyl alcohol (C₄H₁₀O) produced by Nanjing Chemical Reagent Co. LTD were used. Tetraethyl orthosilicate (TEOS, C₈H₂₀O₄Si) produced by Shanghai Maclin Biochemical Technology Co., LTD was used. Absolute ethyl alcohol (C₂H₆O) and ammonium hydroxide (NH₄OH) produced by Shanghai Jiuyi Chemical Reagent Co., LTD were used. All reagents were analytically pure.

2.2 Preparation of nano-samples

2.2a Preparation steps of WO₃:Eu³⁺ nanoparticles: Figure 1 shows the preparation flowchart of WO₃:Eu³⁺ nanoparticles. A quantity of 1.144 g CTAB was dissolved in 50 ml *n*-butanol solution. Europium nitrate, 0.288 g, powder was dissolved in 10 ml distilled water and stirred until dissolved. The above solutions are mixed to obtain a solution of europium nitrate, and solution A was obtained. Ammonium paratungstate particles, 4.8 g, were dissolved in 50 ml distilled water and stirred until dissolved to make a clarified aqueous solution. Then slowly dropped into europium nitrate solution, placed in a 90°C water bath, heating and stirring continuously for 4 h, and solution B was obtained. The remaining solution was poured into the crucible and dried at 100°C for 4 h. The white powder was obtained. Then place it into a muffle furnace to dry and heat it up to 600°C. After drying for 4 h, it was cooled to room temperature with furnace temperature to obtain yellow-green tungsten oxide (WO₃:Eu³⁺) doped with Eu ion powder and then ground and collected.

2.2b Preparation of WO₃:Eu³⁺@SiO₂ nanocomposite: Figure 2 shows the preparation flowchart of WO₃:Eu³⁺@SiO₂ nanoparticles. TEOS was dissolved in 36 ml of anhydrous ethanol, and the content of TEOS was 1, 3, 5 and 7% under alkaline conditions, respectively. A quantity of 0.3 g WO₃:Eu³⁺ powder was dissolved in 72 ml deionized water, and TEOS solution was added to WO₃ solution drop by drop according to different contents. Then the pH value was adjusted to 10 under the alkaline condition of NH₃·H₂O. The stirring rate was 1000 r min⁻¹ at room temperature and pressure, and the reaction lasted for 12 h. To obtain pure WO₃:Eu³⁺@SiO₂ nanocomposites, ultrasonic was used to clean them with anhydrous ethanol twice, followed by centrifugation with a high-speed centrifuge. After centrifugation, the upper clear liquid was poured out, and the lower solid was taken out. The obtained solid was put into the crucible and dried at 90°C in the air-blast drying oven until it was solid. After 3 h, it was removed to be cooled and then ground in the mortar into dense powder; the WO₃:Eu³⁺@SiO₂ nanocomposite was obtained.

WO₃:Eu³⁺, 0.3 g, samples were dissolved in 12, 24, 36 and 72 ml deionized water, respectively. A quantity of 9 ml TEOS was dissolved in 36 ml anhydrous ethanol.

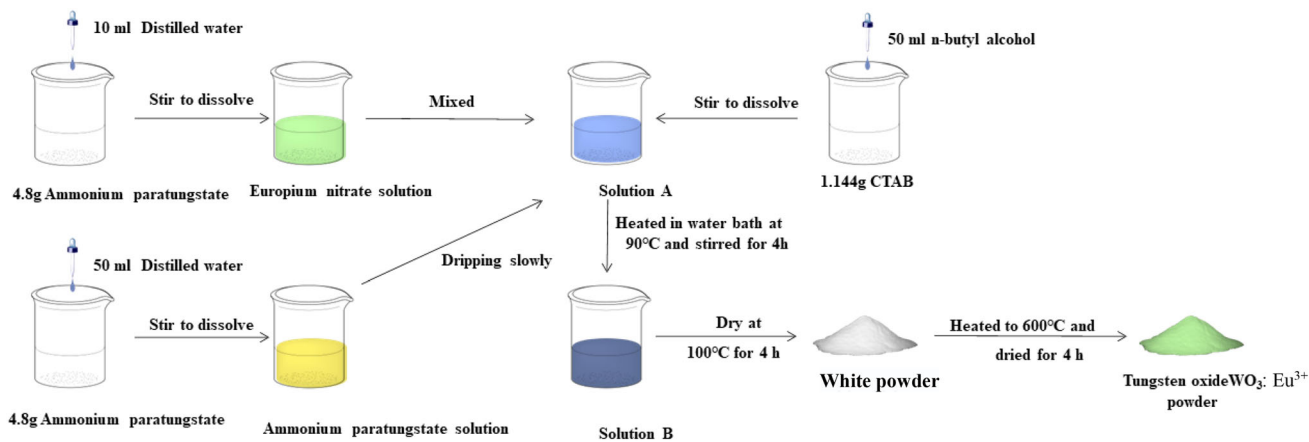


Figure 1. Preparation flowchart of $WO_3:Eu^{3+}$ nanoparticles.

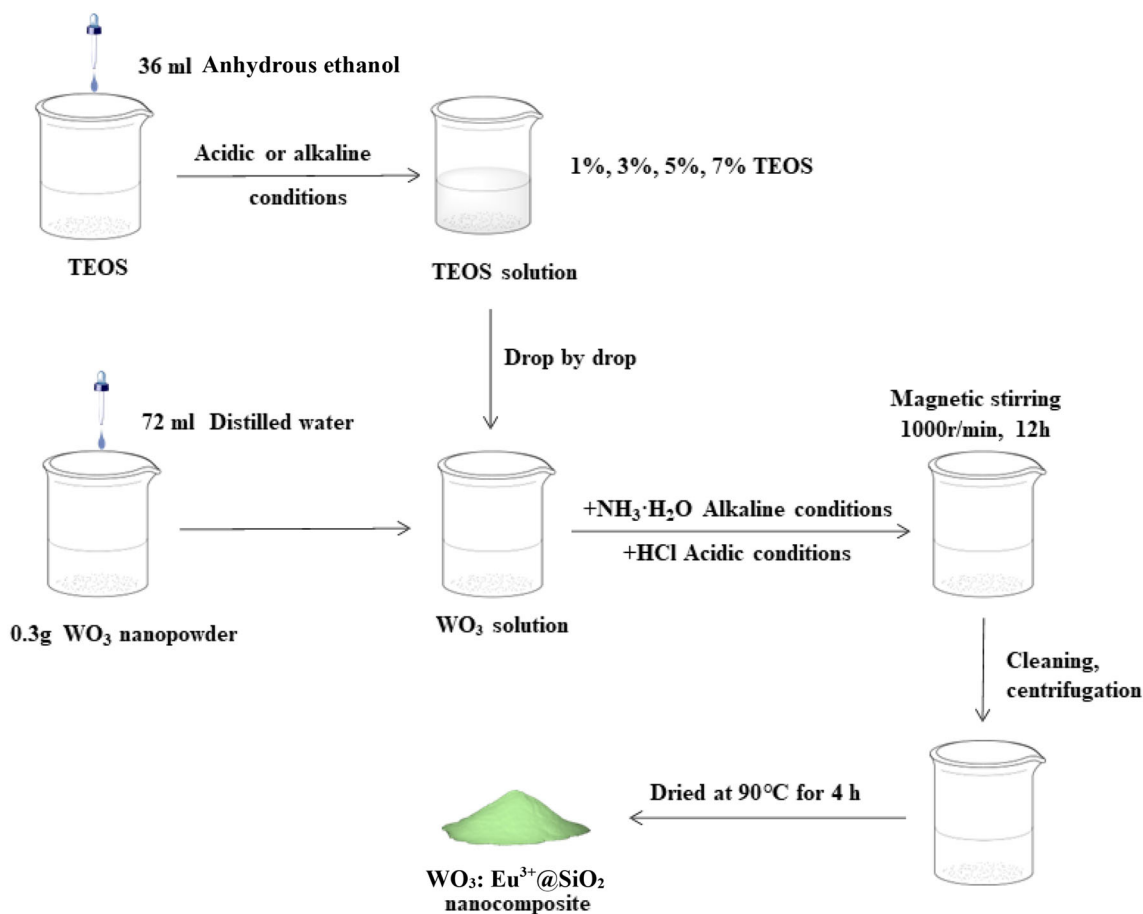


Figure 2. Preparation flowchart of $WO_3:Eu^{3+}@SiO_2$ nanocomposite.

Then it was slowly added into $WO_3:Eu^{3+}$ solutions with different water contents, and the pH was adjusted to 10 with ammonia and stirred on a magnetic stirrer at 90°C for 4 h. To obtain pure $WO_3:Eu^{3+}@SiO_2$ nanocomposites, ultrasonic was used to clean them with anhydrous ethanol twice, followed by centrifugation with a high-

speed centrifuge. After centrifugation, the upper clear liquid was poured out, and the lower solid was taken out. The obtained solid was put into the crucible and dried at 90°C in the air-blast drying oven until it was solid. And then, ground in the mortar into dense powder, the prepared $WO_3:Eu^{3+}@SiO_2$ nanocomposite was obtained.

2.3 Microstructure and morphology characterization of the prepared $\text{WO}_3:\text{Eu}^{3+}@\text{SiO}_2$ nanocomposite

The microstructure of the prepared $\text{WO}_3:\text{Eu}^{3+}@\text{SiO}_2$ nanocomposite sample was characterized by a D8 Advance X-ray diffractometer (XRD). According to the measured data, phase analysis was performed in Jade software, and the substances contained in the sample were determined using PDF cards. The instrument voltage was set to 20 kV, the current to 5 mA, the Angle range from 2° to 80° , the residence time was 0.1 s, the step length 0.02° , and the speed at $12^\circ \text{ min}^{-1}$.

Morphology of the prepared $\text{WO}_3:\text{Eu}^{3+}$ and $\text{WO}_3:\text{Eu}^{3+}@\text{SiO}_2$ nanocomposite samples was observed by Merlin Compact scanning electron microscope (SEM). Nano Measurer software was used to measure the particle size of the SEM images. The instrument's resolution was High Vacuum mode $1.0\text{nm}@15\text{kV}$ $\text{WD} = 2 \text{ nm}$, the magnification ranged from 12 to 2 million times, the sample current ranged from 5 Pa to 20 nA, and the acceleration voltage ranged from 0.05 to 30 kV.

2.4 Fluorescence spectra of the prepared $\text{WO}_3:\text{Eu}^{3+}@\text{SiO}_2$ nanocomposite

FS5 steady-state/unsteady fluorescence spectrometer was used to test the prepared samples' luminescence under different TEOS and water content. The excitation light source was a deuterium lamp, the signal-to-noise ratio (SNR) was 600:1, the test step size was 1 nm, and the standing time was 0.5 s.

3. Results and discussion

3.1 Microstructure analysis of the prepared $\text{WO}_3:\text{Eu}^{3+}@\text{SiO}_2$ nanocomposite

Figure 3a shows XRD images of the prepared $\text{WO}_3:\text{Eu}^{3+}@\text{SiO}_2$ nanocomposite with different contents of Si. Compared with the standard JCPDS card, it can be seen that the diffraction peaks of the prepared samples at 22.9° , 23.5° , 24.1° , 28.6° and 33.9° correspond to (002), (020), (200), (111) and (202), respectively. These diffraction peaks correspond to the same peaks on PDF#72-1465 standard card of monocline WO_3 , indicating that the prepared sample is WO_3 powder, the space group is $\text{P}21/n(14)$, and its cell parameters are $a = 7.301$, $b = 7.530$, $c = 7.680$, $\alpha = \beta = \gamma = 90^\circ$. The other phases of the samples are basically consistent with the PDF-43-1008 standard card of Eu_2O_3 in the cubic crystal system. The parameters are $a = b = c = 10.868 \text{ \AA}$, $\alpha = \beta = \gamma = 90^\circ$, which belong to the space group $\text{I}a3(206)$. As can be seen from figure 3a, the diffraction peak crystal and microstructure of the prepared samples do not change before and after the encapsulation of SiO_2 . With the

increase of TEOS content, the XRD pattern keeps increasing, so it can be inferred that SiO_2 exists in the form of amorphous. In addition, the diffraction peaks of the nanopowders were almost the same before and after being coated with SiO_2 , indicating that changing the content of TEOS has little effect on the intensity of the diffraction peaks.

The full-width at half-maximum (FWHM) and grain size of the prepared samples were obtained by the Scherrer formula and shown in figure 3b. It shows that the average FWHM is inversely proportional to the average grain size. The larger the half-width is, the smaller the grain size is. With the increase of TEOS content, the grain size first decreases, then increases and then decreases. The average particle sizes of the prepared nanocomposites with 1, 3, 5 and 7% TEOS content are 11.6, 13.7, 10.9 and 13.5 nm, respectively. The grain size is the smallest when TEOS content is 5%, and the grain size is the largest when TEOS content is 3%.

Figure 4a shows XRD patterns of the prepared $\text{WO}_3:\text{Eu}^{3+}@\text{SiO}_2$ nanocomposite under alkaline conditions with different water–alcohol ratios ($\text{H}_2\text{O}:\text{C}_2\text{H}_6\text{O}$). After phase retrieval, diffraction peaks were found on the (002), (020), (200), (120) and (202) crystal planes corresponding to 23.2° , 23.7° , 24.4° , 26.7° and 34.2° , respectively. It is consistent with the peak on PDF#72-1465 standard card of monoclinic WO_3 , indicating that the sample is WO_3 nanopowder. The other phases of the samples are basically consistent with the PDF-43-1008 standard card of Eu_2O_3 in the cubic crystal system. The parameters are $a = b = c = 10.868 \text{ \AA}$, $\alpha = \beta = \gamma = 90^\circ$, which belongs to the space group $\text{I}a3(206)$. Meanwhile, the doped TEOS is not evident in the diffraction peak, which also indicates that SiO_2 wraps $\text{WO}_3:\text{Eu}^{3+}$ in an amorphous form. The spatial group of the sample is $\text{P}21/N(14)$, and its cell parameters are $a = 7.306$, $b = 7.540$, $c = 7.692$, $\alpha = \beta = \gamma = 90^\circ$. It can be seen from figure 4a that the water–alcohol ratio has a significant influence on the diffraction peak intensity. When the water–alcohol ratio is 2:1, the diffraction peak intensity is close to that of pure $\text{WO}_3:\text{Eu}^{3+}$ nanopowder; when the water–alcohol ratio is 1:1.5, the diffraction peak intensity is weaker than that of pure $\text{WO}_3:\text{Eu}^{3+}$ powder.

The grain size and FWHM of the prepared $\text{WO}_3:\text{Eu}^{3+}@\text{SiO}_2$ nanocomposites with different water–alcohol ratios were calculated by the Scherrer formula and given in figure 4b. It can be found that the grain size of the prepared samples is inversely proportional to FWHM. With the increase of water content, the grain size of the sample decreases first, then increases and then decreases. Under the condition that the TEOS content remains unchanged, the grain size reaches its maximum when the water–alcohol ratio is 1:3, and the SiO_2 shell coated with prepared WO_3 becomes thicker. The intensity of the prepared WO_3 diffraction peak is weakened. This corresponds to the weakening of the prepared WO_3 diffraction peak of the prepared $\text{WO}_3:\text{Eu}^{3+}@\text{SiO}_2$ nanocomposite with the water–alcohol ratio of 1:3 in figure 3b.

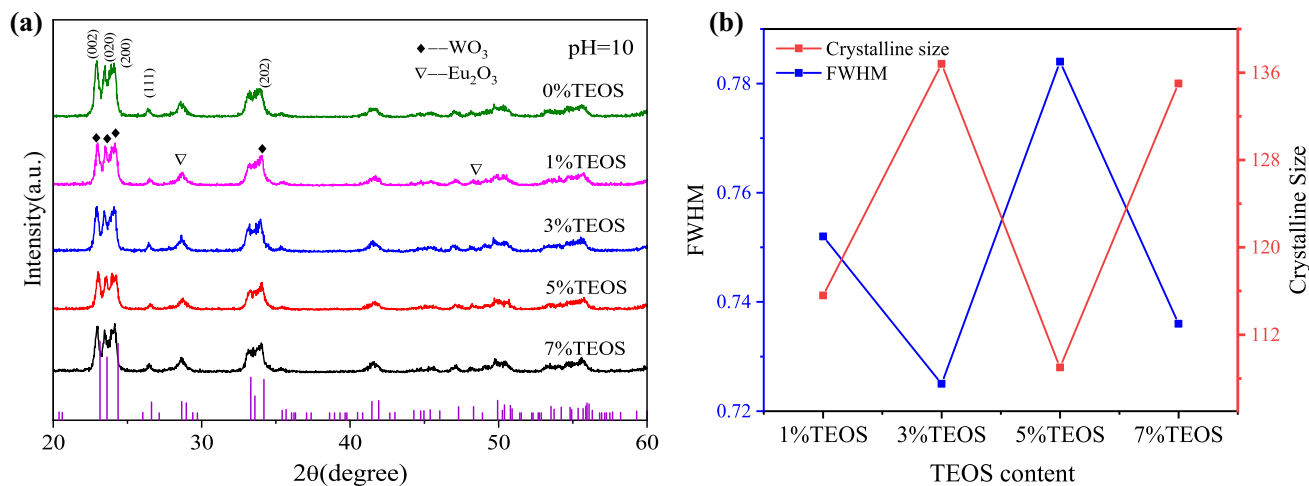


Figure 3. (a) XRD patterns, (b) grain size and FWHM of the prepared $WO_3:Eu^{3+}$ sample and $WO_3:Eu^{3+}@SiO_2$ nanocomposite under alkaline conditions with different TEOS contents.

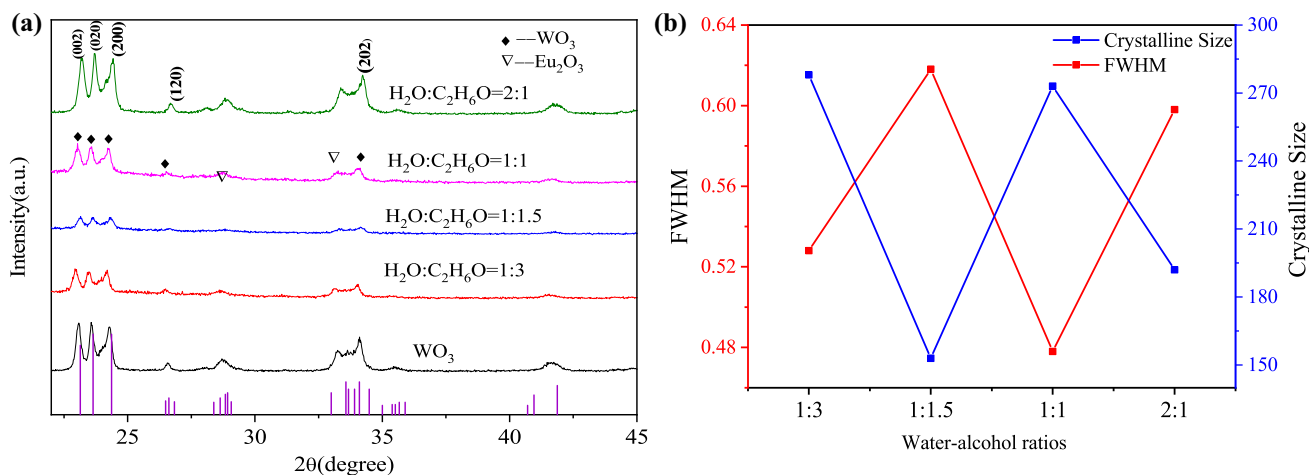


Figure 4. (a) XRD patterns, (b) grain size and FWHM of the prepared $WO_3:Eu^{3+}$ sample and $WO_3:Eu^{3+}@SiO_2$ nanocomposite under alkaline conditions with different water–alcohol ratios ($H_2O: C_2H_5OH$).

3.2 Morphology of the prepared $WO_3:Eu^{3+}@SiO_2$ nanocomposite

Figure 5 shows SEM images of the prepared $WO_3:Eu^{3+}$ sample (a), $WO_3:Eu^{3+}@SiO_2$ nanocomposites with TEOS content of 1 (b), 3 (c), 5 (d) and 7% (e). The above XRD analysis shows that the prepared $WO_3:Eu^{3+}@SiO_2$ nanocomposites are monoclinic crystal phases. Figure 5a shows the SEM image of pure $WO_3:Eu^{3+}$ nanopowder, and it can be seen that many particles are connected to each other and are roughly spherical. Due to tungsten oxide after heat treatment, it is the process of organic decomposition and water loss. The loss of water leads to the bonding of surface-active groups of different particles, which leads to the agglomeration of tungsten oxide particles. Figure 5b, c, d and e shows that grain size increases significantly with the increase of TEOS content. Many nanoparticles of varying sizes are piled on top of each other irregularly. Using Nano

Measurer software, the grain size of the samples is calculated. The average grain size of the prepared samples is 71.5 nm of the prepared $WO_3:Eu^{3+}$ sample, 91.6 nm of the prepared $WO_3:Eu^{3+}@SiO_2$ nanocomposites with 1% TEOS, 89.8 nm of 3% TEOS, 95.5 nm of 5 % TEOS and 105.3 nm of 7% TEOS, respectively. The sample size with 7%TEOS content is the largest, followed by 5%TEOS. The prepared $WO_3:Eu^{3+}$ sample without SiO_2 modification has the smallest size. Figure 5f–j shows that grain size increases significantly with the increase of water–alcohol ratios. The results show that the prepared $WO_3:Eu^{3+}@SiO_2$ nanocomposites are spherical and granular, and the average particle size is below 100 nm.

Figure 6 shows TEM image of the synthesized $WO_3:Eu^{3+}@SiO_2$ nanocomposite, the diffraction pattern of WO_3 , and the high-resolution TEM image of $WO_3:Eu^{3+}@SiO_2$ nanocomposite taken along [312] direction. The high-resolution TEM image shows the lattice fringes of WO_3 as 0.31 and 0.35 nm in the (112) and (021) planes, respectively. It is

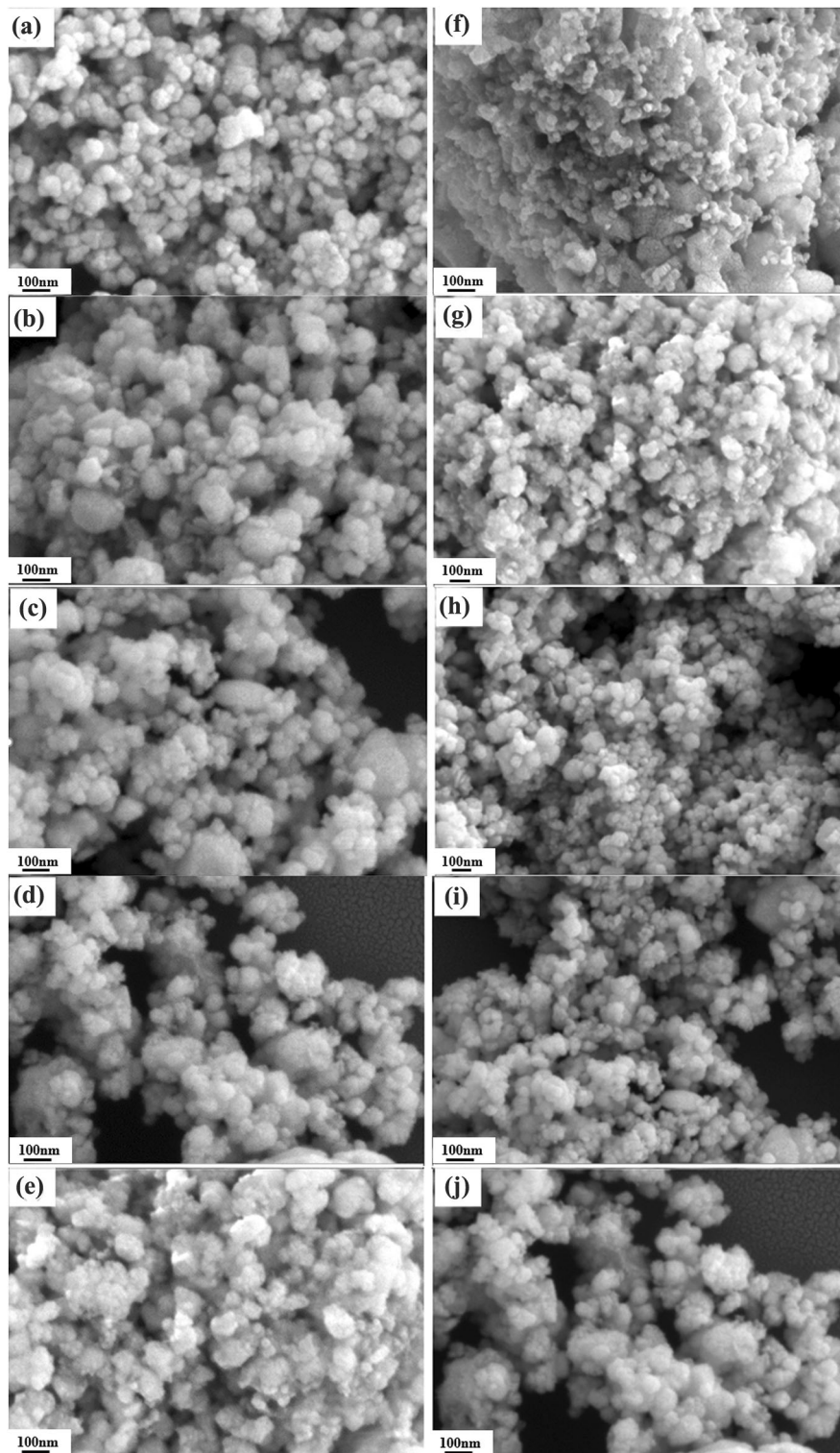


Figure 5. SEM images of the (a) prepared $\text{WO}_3:\text{Eu}^{3+}$ sample, $\text{WO}_3:\text{Eu}^{3+}@\text{SiO}_2$ nanocomposites with different TEOS content of (b) 1%, (c) 3%, (d) 5%, (e) 7% and (f) the prepared $\text{WO}_3:\text{Eu}^{3+}$ sample with different water-alcohol ratios of (g) 1:3, (h) 1:1.5, (i) 1:1 and (j) 2:1.

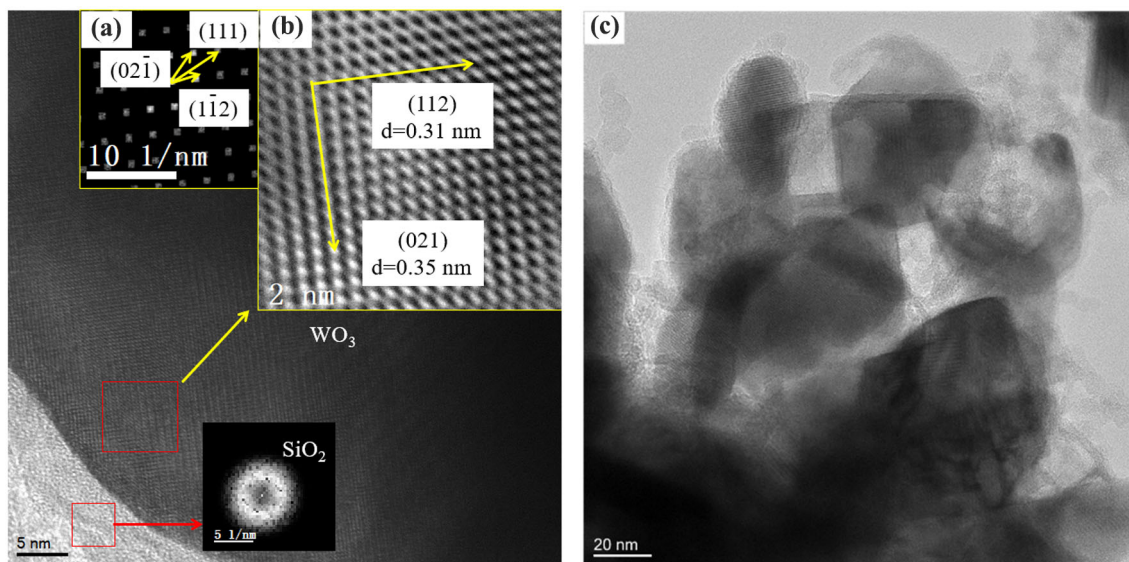


Figure 6. TEM image of $WO_3:Eu^{3+}@SiO_2$ nanocomposite, (a) diffraction pattern, (b) high-resolution TEM image of $WO_3:Eu^{3+}@SiO_2$ nanocomposite taken along [312] direction, (c) low-magnification TEM image.

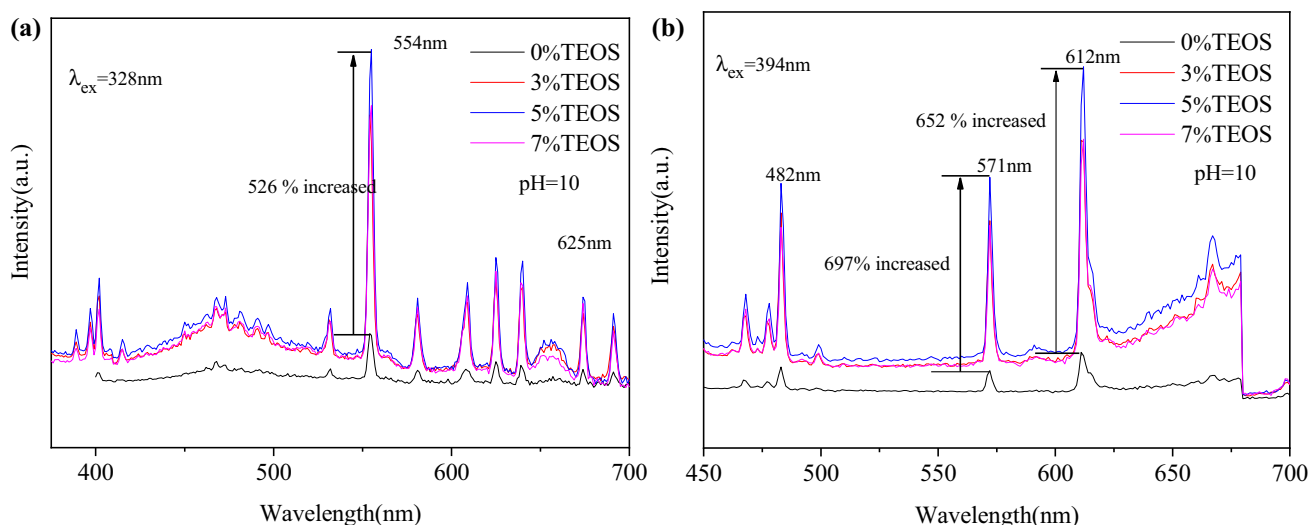


Figure 7. Emission spectra of the prepared $WO_3:Eu^{3+}$ sample and $WO_3:Eu^{3+}@SiO_2$ nanocomposites with different TEOS contents under alkaline conditions at (a) 328 nm and (b) 394 nm excitation wavelength.

found that the black part is WO_3 and the other part is inorganic SiO_2 .

3.3 Luminescence properties of the prepared $WO_3:Eu^{3+}@SiO_2$ nanocomposites

3.3a Emission spectra: Figure 7a shows the emission spectra of the prepared $WO_3:Eu^{3+}$ sample and $WO_3:Eu^{3+}@SiO_2$ nanocomposites with different TEOS contents under alkaline conditions excited at 328 nm. When the excitation wavelength is 328 nm, the highest emission peak of $WO_3:Eu^{3+}@SiO_2$ nanocomposite is at 554 nm, which is in the range of green light band originating from the

$^5D_1 \rightarrow ^7F_1$. The luminescence intensity of the sample with 5% TEOS content is the highest, which is 526% higher than that of the $WO_3:Eu^{3+}$ powder before modification. The luminescence intensity of the sample with 3% TEOS content is the lowest.

Figure 7b shows the emission spectra of the prepared $WO_3:Eu^{3+}$ sample and $WO_3:Eu^{3+}@SiO_2$ nanocomposites with different TEOS contents under alkaline conditions excited at 394 nm. There are three obvious emission peaks at 394 nm, a red emission peak at 612 nm, an orange emission peak at 571 nm, and a blue emission peak at 482 nm. The emission peak at 612 nm is the strongest, and the emission intensity of the prepared $WO_3:Eu^{3+}@SiO_2$ nanocomposites with 5% TEOS content is 652% higher than

that of the prepared $\text{WO}_3:\text{Eu}^{3+}$ sample. When the excitation wavelength is 571 nm, the luminescence intensity of the prepared nano- $\text{WO}_3:\text{Eu}^{3+}@\text{SiO}_2$ composites with 5% TEOS content is 697% higher than that of the prepared $\text{WO}_3:\text{Eu}^{3+}$ sample. The main reasons are two aspects. First, the fluorescence enhancement of WO_3 particles coated by SiO_2 shell is mainly due to the localized surface plasmon resonance effect of metal oxide nanoparticles; second, the enhancement of fluorescence by shell thickness is not linear. With the increase of amorphous SiO_2 thickness, the scattering and absorption of light by the shell increase. Therefore, the fluorescence intensity of 7% TEOS is less than that of 5% TEOS [22–24].

Under the excitation of different wavelengths, the strongest emission peak is at 554 nm at the wavelength of 328 nm, and the emission peak is in the green-light band. In the emission spectrum excited at 394 nm, the peak is at 612 nm, which is in the red-light band originating from the ${}^5\text{D}_0 \rightarrow {}^7\text{F}_2$ belonging to an electric dipole transition. The emission peak intensity and luminescence intensity of the prepared $\text{WO}_3:\text{Eu}^{3+}@\text{SiO}_2$ nanocomposites with 5% TEOS content are the strongest both at 328 and 394 nm.

Figure 8a shows emission spectra of the prepared $\text{WO}_3:\text{Eu}^{3+}$ sample and $\text{WO}_3:\text{Eu}^{3+}@\text{SiO}_2$ nanocomposites with different water–alcohol ratios at 328 nm excitation wavelength. There are three obvious emission peaks at 401, 554 and 655 nm, among which the highest emission peak is located at 401 nm. The emission peak intensity of the prepared sample with the water–alcohol ratio of 1:3 is the strongest, and the emission intensity is 669% higher than that of the prepared sample with the water–alcohol ratio of 2:1. The emission peak intensity of the sample with water–alcohol ratio of 1:1.5 is the next, and the emission peak intensity of the sample with water alcohol ratio of 2:1 is the worst.

Figure 8b shows emission spectra of the prepared $\text{WO}_3:\text{Eu}^{3+}$ sample and $\text{WO}_3:\text{Eu}^{3+}@\text{SiO}_2$ nanocomposites with different water–alcohol ratios at 394 nm excitation wavelength. There are three obvious emission peaks at 483, 572 and 611 nm, among which the highest emission peak is located at 611 nm. At this time, the emission peak intensity of the prepared sample with the water–alcohol ratio of 1:3 is 138% higher than that of the prepared sample with the water–alcohol ratio of 2:1. The emission peak is located at 572 nm, and the emission peak intensity of the prepared sample with water–alcohol ratio of 1:3 is 146% higher than that of the prepared sample with water–alcohol ratio of 2:1. The sample with the same water–alcohol ratio of 1:3 has the strongest emission peak intensity, followed by the sample with the water–alcohol ratio of 1:1.5, and the sample with the water–alcohol ratio of 2:1 has the worst emission peak intensity.

3.3b Excitation spectra: Figure 9 shows excitation spectra of nanoparticles with different TEOS contents in alkaline conditions (a) and water–alcohol ratios (b) at 612 nm monitoring wavelength. It can be seen that there is a relatively weak peak of 328 nm in the excitation spectrum, which is mainly due to the charge transfer between W–O and Eu–O [25]. Several characteristic peaks between 350 and 550 nm belong to the transition of ${}^7\text{F}_0 \rightarrow {}^5\text{D}_1$ of Eu^{3+} . Peaks mainly located at 362, 394, 422, 465 and 499 nm, each corresponding to the transition of ${}^7\text{F}_0 \rightarrow {}^5\text{D}_4$, ${}^7\text{F}_0 \rightarrow {}^5\text{L}_6$, ${}^7\text{F}_0 \rightarrow {}^5\text{D}_3$, ${}^7\text{F}_0 \rightarrow {}^5\text{D}_2$ and ${}^7\text{F}_0 \rightarrow {}^5\text{D}_1$, respectively. The maximum peak was at 499 nm, belonging to the transition of ${}^7\text{F}_0 \rightarrow {}^5\text{D}_1$. Figure 8a shows that the luminescence intensity increases significantly after TEOS is added. The luminescence intensity of the sample is the strongest when TEOS is 5%, and the sample's strongest characteristic peak is located at 499 nm. Figure 8b shows that the luminescence intensity is the strongest when the water–alcohol ($\text{H}_2\text{O}:\text{C}_2\text{H}_5\text{OH}$) ratio is 1:3, and the strongest characteristic peak is also located at 499 nm of the sample.

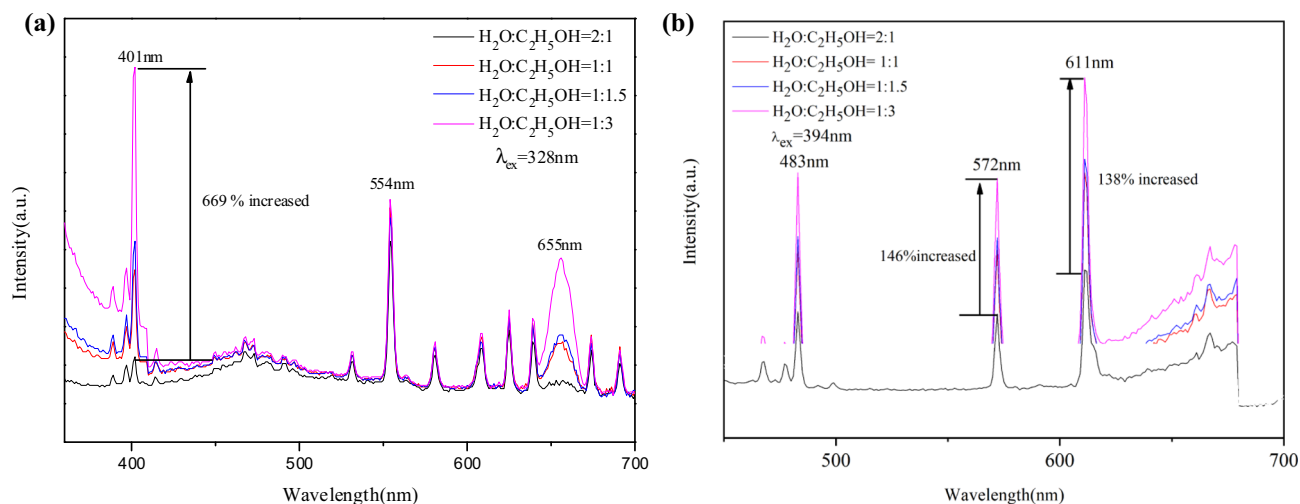


Figure 8. Emission spectra of the prepared $\text{WO}_3:\text{Eu}^{3+}$ sample and $\text{WO}_3:\text{Eu}^{3+}@\text{SiO}_2$ nanocomposites with different water–alcohol ratios ($\text{H}_2\text{O}:\text{C}_2\text{H}_5\text{OH}$) at (a) 328 nm and (b) 394 nm excitation wavelength.

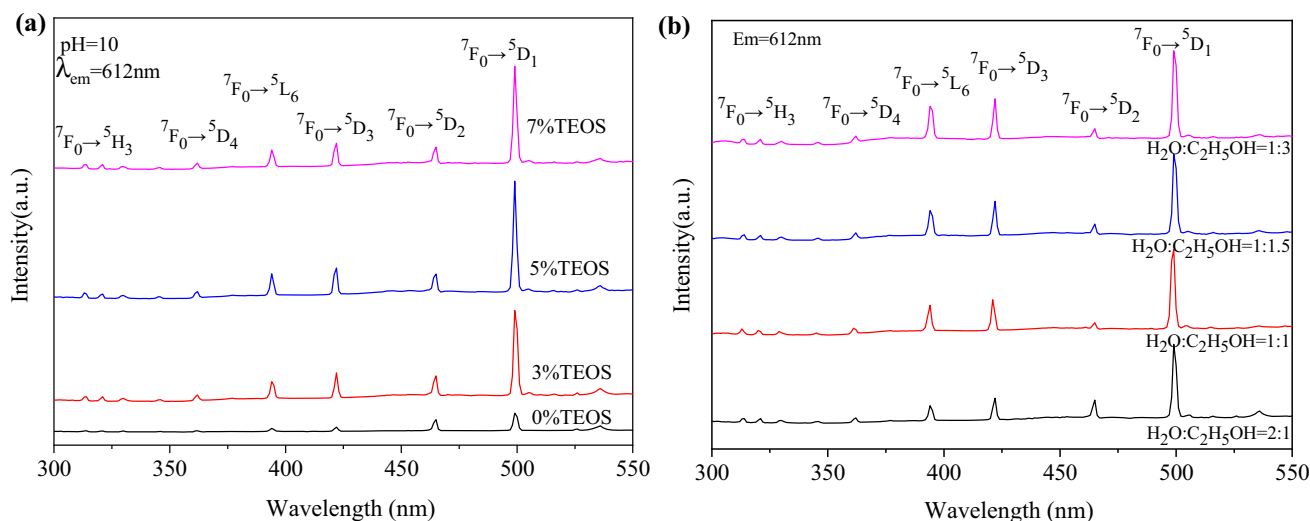


Figure 9. Excitation spectra of nanoparticles with different TEOS contents in (a) alkaline condition and (b) water–alcohol ratios ($\text{H}_2\text{O}:\text{C}_2\text{H}_5\text{OH}$), at 612 nm monitoring wavelength.

4. Conclusion

$\text{WO}_3:\text{Eu}^{3+}$ powder was prepared by microemulsion method with cetyltrimethyl ammonium bromide (CTAB) as the surfactant. The prepared $\text{WO}_3:\text{Eu}^{3+}$ samples were wrapped with SiO_2 by a coating method. The $\text{WO}_3:\text{Eu}^{3+}@\text{SiO}_2$ nanocomposites with the core-shell structure were prepared by controlling TEOS content (1, 3, 5 and 7%) and water–alcohol ratio (1:3, 1:1.5, 1:1 and 2:1). The structure, morphology and luminescence properties of the prepared $\text{WO}_3:\text{Eu}^{3+}@\text{SiO}_2$ samples were characterized by XRD, SEM, TEM and fluorescence spectra. The results show that the prepared $\text{WO}_3:\text{Eu}^{3+}@\text{SiO}_2$ nanocomposites are spherical and granular, and the average particle size is below 100 nm. Under the condition of different TEOS contents, the strongest characteristic peak is located at 554 nm in the green-light band at the excitation wavelength of 328 nm. Under the condition of 5% TEOS content, the luminescence intensity of the prepared $\text{WO}_3:\text{Eu}^{3+}@\text{SiO}_2$ composites is the highest, which increases by 526%. Under different water–alcohol ratio conditions, the prepared $\text{WO}_3:\text{Eu}^{3+}@\text{SiO}_2$ nanocomposite has the strongest luminescence intensity at the water–alcohol ratio of 1:3, and the excitation wavelength is 328 nm. The emission peak intensity of the prepared $\text{WO}_3:\text{Eu}^{3+}@\text{SiO}_2$ sample with the water–alcohol ratio of 1:3 is the strongest, and the intensity is 669% higher than that of the water–alcohol ratio of 2:1.

Acknowledgements

We are supported by the Natural Science Foundation of the Jiangsu Higher Education Institutions of China, Grant/Award Number: 22KJD430007; the Opening Project of Jiangsu Key Laboratory of Advanced Structural Materials

and Application Technology, Grant/Award Number: ASMA202202; Jiangsu Province Industry-University-research cooperation Project, Grant/Award Number: BY2022095; Jinling University of Science and Technology, Grant/Award Number: jit-b-201824; Jinling Institute of Science and Technology Incentive Fund, Grant/Award Number: Jit-fhxm-201921.

References

- [1] Cargnello M, Wieder N L, Montini T, Gorte J R and Fornasiero P 2010 *J. Am. Chem. Soc.* **132** 1402
- [2] Cargnello M, Jaén J D, Garrido J C H and Fornasiero P 2012 *Science* **337** 713
- [3] Sun X and Li Y 2004 *Angew. Chem.* **116** 607
- [4] Yin Y, Rioux R M, Erdonmez C K, Hughes S, Somorjai G A and Alivisatos A P 2004 *Science* **304** 711
- [5] Joo S H, Park J Y, Tsung C K, Yamada Y, Peidong Y and Somorjai G A 2009 *Nat. Mater.* **8** 126
- [6] Sivakumar S, Diamente P R and van Veggel F C J M 2006 *Chem. – Eur. J.* **12** 5878
- [7] Li S, Zhang M, Zhan Z, Liu R and Xiong X 2020 *J. Magn. Mag. Mater.* **500** 166321
- [8] Dou J, Chen B, Liu G, Dong X and Zhu J 2022 *J. Rare Earth* **40** 193
- [9] Lin C, Sun K, Zhang C, Tan T and Whittaker A 2020 *Microporous Mesoporous Mater.* **293** 109775
- [10] Kulp C, Chen X, Puschhof A, Schwamborn S, Somsen S, Schumann *et al* 2010 *ChemPhysChem* **11** 2854
- [11] Stöber W, Fink A and Bohn E 1968 *J. Colloid Interface Sci.* **26** 62
- [12] Rao K S, El-Hami K, Kodaki T, Matsushige K and Makino K 2005 *J. Colloid Interface Sci.* **289** 125
- [13] Gorobtsov P, Simonenko T L and Simonenko N P 2021 *Russ. J. Inorg. Chem.* **66** 1811
- [14] Deepa B and Rajendran V 2018 *Nano-struct. Nano-Object* **16** 185

- [15] Martínez D S, Martínez-De La Cruz A and Cuéllar E L 2011 *Appl. Catal. A Gen.* **398** 179
- [16] Khosravi H B, Rahimi R and Rabbani M 2021 *Silicon* **13** 451
- [17] Dutov V V, Mamontov G V, Zaikovskii V I, Liotta L F and Vodyankina O V 2018 *Appl. Catal. B Environ.* **221** 598
- [18] Areerob Y, Cho J Y, Jang W K and Oh W C 2018 *Ultrason. Sonochem.* **41** 267
- [19] Khalid B, Rahim A, Gilani M A, Younus A R, Tabassum S, Iqbal J *et al* 2018 *J. Mol. Liq.* **4** 450
- [20] Bian X 2018 *J. Supercond. Nov. Magn.* **31** 3685
- [21] Khoshnam M and Salimijazi H 2021 *Surf. Interfaces* **26** 101322
- [22] Xu D D, Deng Y L, Li C Y, Lin Y and Tang H W 2017 *Biosens. Bioelectron.* **87** 881
- [23] Ghosh P, Oliva J, Rosa E D L, Haldar K K, Solis D and Patra A 2008 *J. Phys. Chem. C* **112** 9650
- [24] Pushpal G, Arik K and Amitava P 2010 *Nanoscale* **2** 1196
- [25] Feng W, Jin Y, Wu Y, Li D F and Cai A K 2013 *J. Lumin.* **134** 614